Structure and Magnetic Properties of the $AB(HCO_2)_3$ ($A = Rb^+$ or Cs^+, $B = Mn^{2+}$, Co^{2+} or Ni^{2+}) Frameworks: Probing the Effect of Size on the Phase Evolution of the Ternary Formates

Sally M. Bovill[a] and Paul J. Saines[a,b]

[a]Department of Chemistry, University of Oxford
Inorganic Chemistry Laboratory, South Parks Road
Oxford, OX1 3QR

[b]School of Physical Sciences, Ingram Building
University of Kent
Canterbury CT2 7NH

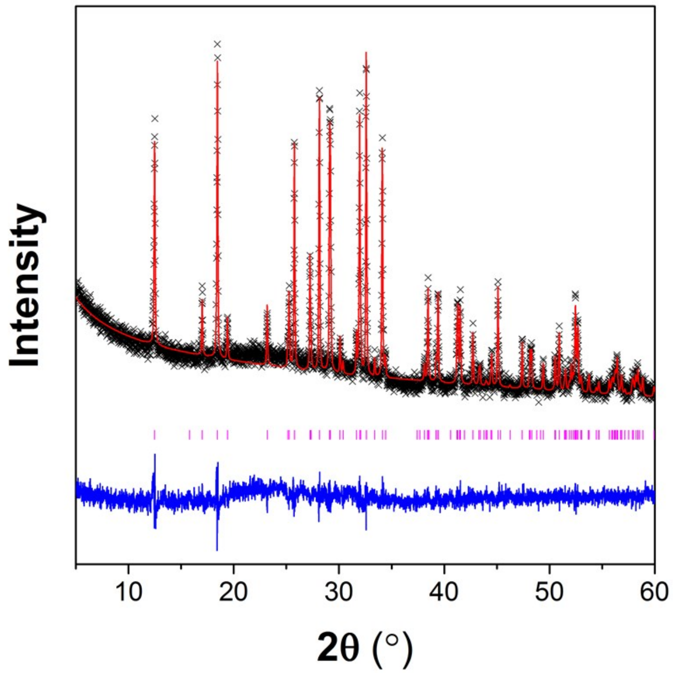

Fig. S1: Powder X-ray diffraction pattern of $RbMn(HCO_2)_3$ fitted using the Le Bail method indicating the purity of the sample. The crosses, red upper line, blue lower line and vertical markers indicate the observed intensity, calculated intensity, difference plot and expected positions of Bragg reflections. The final R_p, R_{wp} and χ^2 values are 5.25 %, 6.64 % and 1.86. The unit cell parameters were determined to be a = 11.2792(4) Å, b = 9.1321(4) Å, c = 7.0992(3) Å and β = 97.31794(2)°.

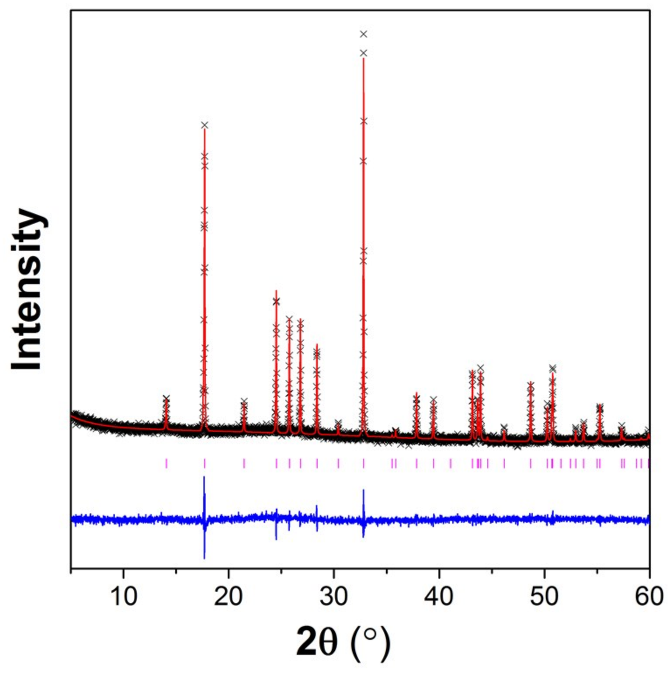

Fig. S2: Powder X-ray diffraction pattern of $RbCo(HCO_2)_3$ fitted using the Le Bail method indicating the purity of the sample. The symbols are the same as in Fig. S1. The final R_p, R_{wp} and χ^2 values are 4.81 %, 6.12 % and 1.48. The unit cell parameters were determined to be a = 7.25486(14) Å and c = 8.27212(20) Å.

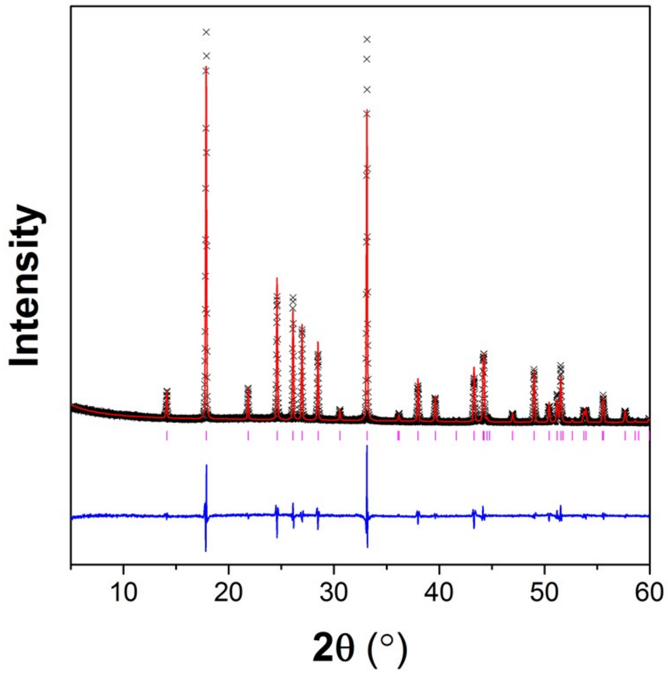

Fig. S3: Powder X-ray diffraction pattern of $RbNi(HCO_2)_3$ fitted using the Le Bail method indicating the purity of the sample. The symbols are the same as in Fig. S1. The final R_p, R_{wp} and χ^2 values are 9.70 %, 12.41% and 4.22. The unit cell parameters were determined to be a = 7.23158(14) Å and c = 8.12833(19) Å.

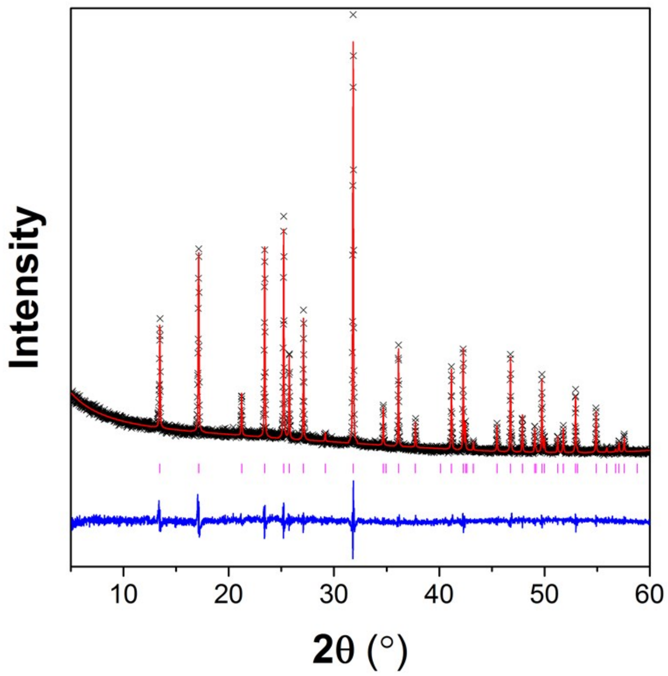

Fig. S4: Powder X-ray diffraction pattern of $CsMn(HCO_2)_3$ fitted using the Le Bail method indicating the purity of the sample. The symbols are the same as in Fig. S1. The final R_p, R_{wp} and χ^2 values are 5.87 %, 7.76 % and 1.98. The unit cell parameters were determined to be a = 7.58858(13) Å and c = 8.36094(18) Å.

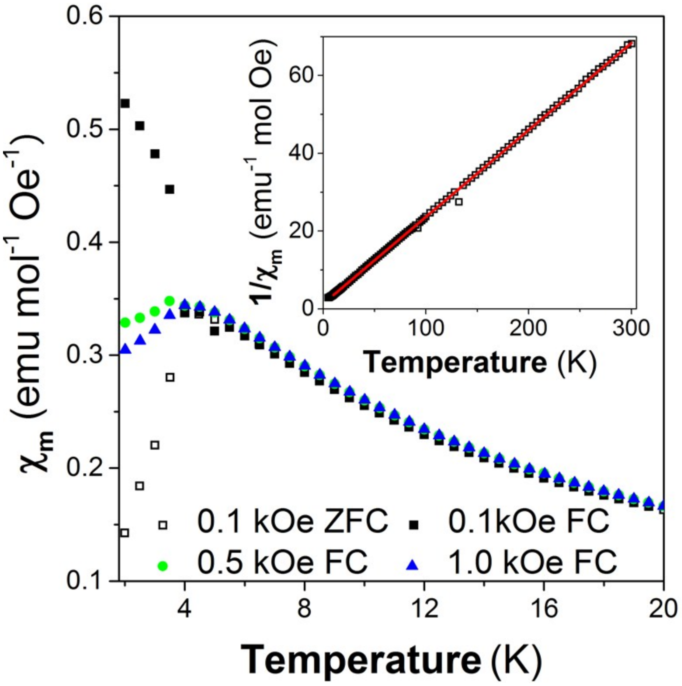

Fig. S5: Plot of variable temperature magnetic susceptibility measurements of $RbMn(HCO_2)_3$ in various magnetic fields with the insert showing the Curie-Weiss fit to the inverse of the 100 Oe ZFC susceptibility measurement measured to a minimum temperature of 5 K.

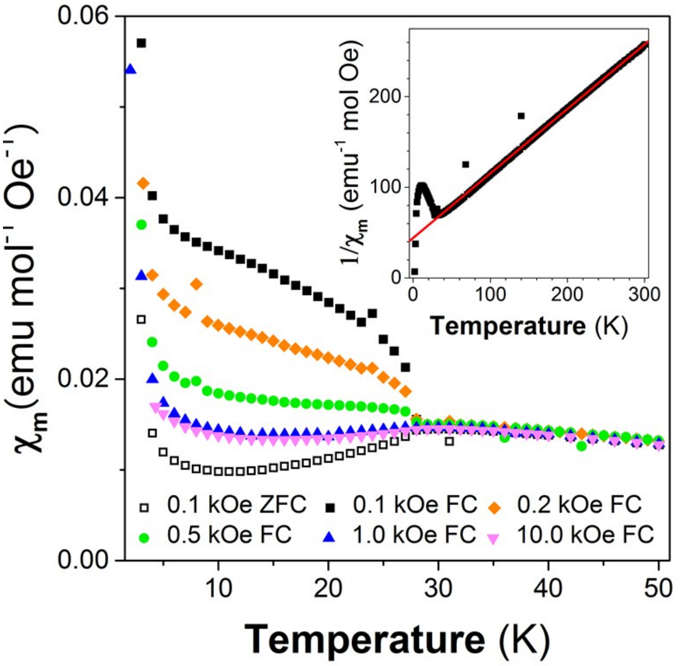

Fig. S6: Plot of variable temperature magnetic susceptibility measurements of $RbNi(HCO_2)_3$ in various magnetic fields with the insert showing the Curie-Weiss fit to the inverse of the 100 Oe ZFC susceptibility measurement above 50 K.

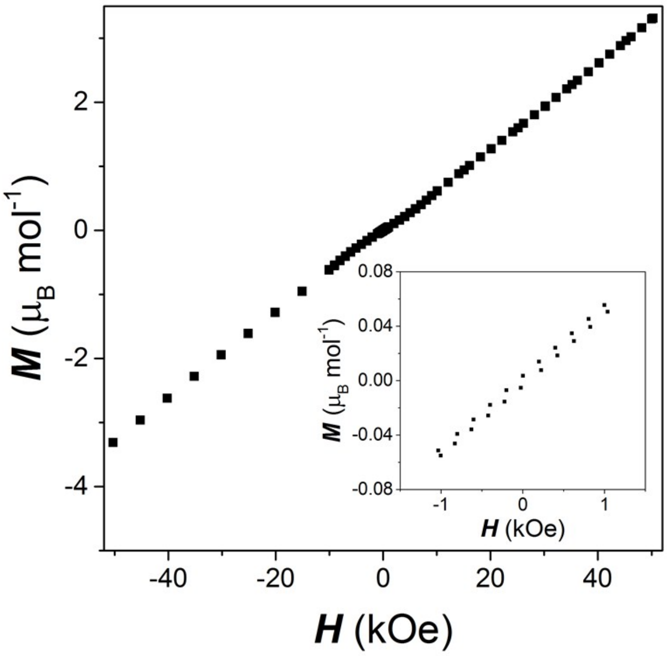

Fig. S7: Isothermal magnetisation measurement on $RbMn(HCO_2)_3$ at 2 K with an insert highlighting the weak hysteresis in low applied fields.

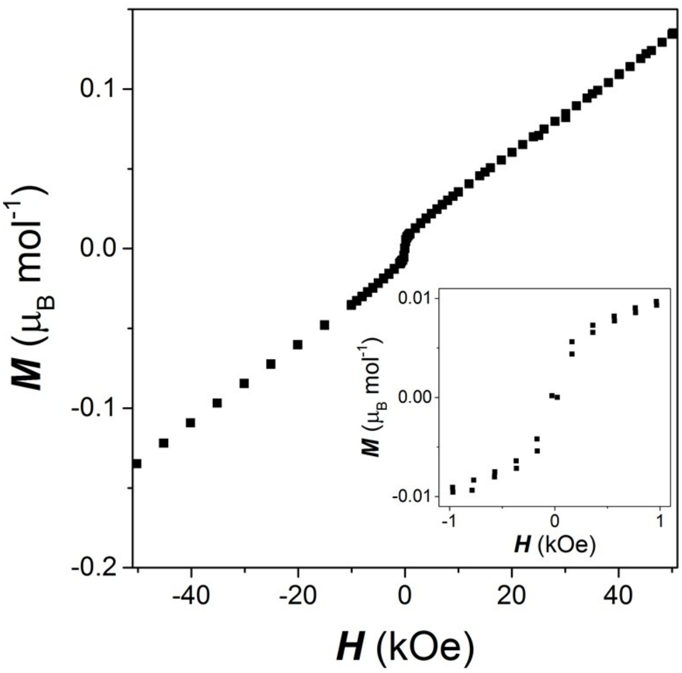

Fig. S8: Isothermal magnetisation measurements on $RbNi(HCO_2)_3$ at 2 K with an insert highlighting the significant hysteresis in low applied fields.

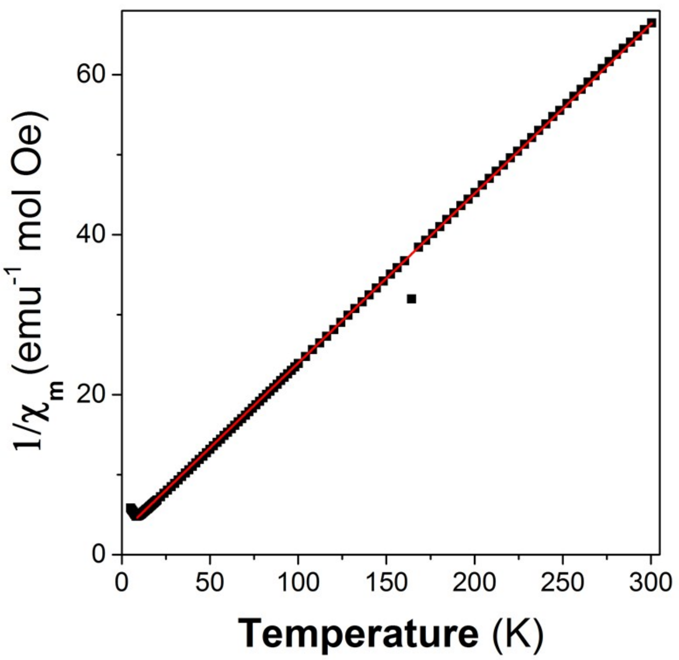

Fig. S9: Curie-Weiss fit to the inverse magnetic susceptibility measurement of $CsMn(HCO_2)_3$ versus temperature above 10 K.

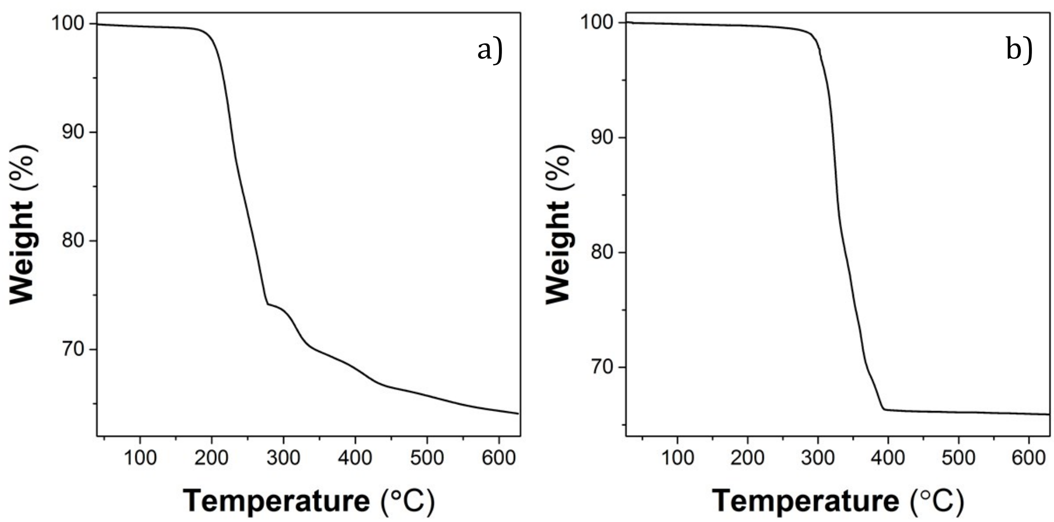

Fig. S10: Thermogravimetric analysis of $RbMn(HCO_2)_3$ in a) air and b) nitrogen.

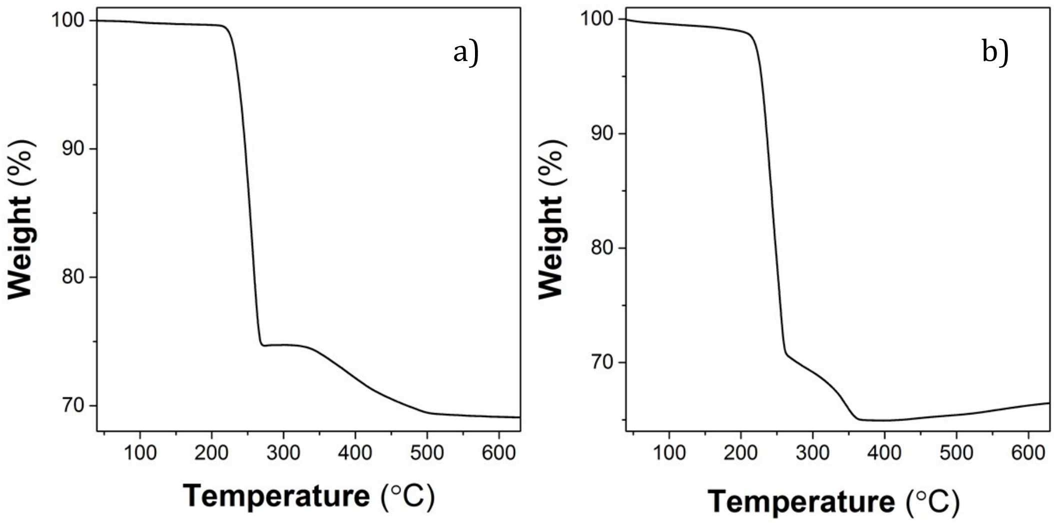

Fig. S11: Thermogravimetric analysis of $RbCo(HCO_2)_3$ in a) air and b) nitrogen.

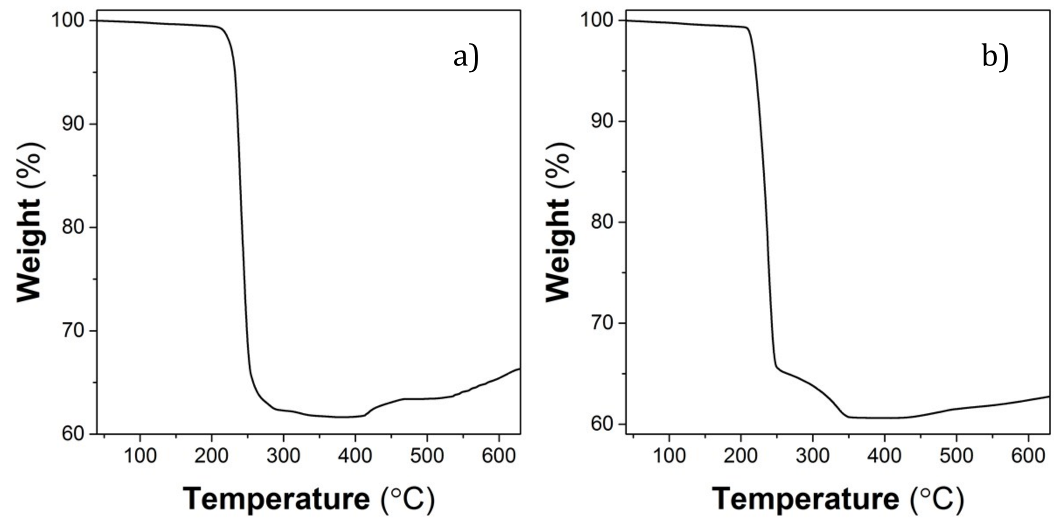

Fig. S12: Thermogravimetric analysis of $RbNi(HCO_2)_3$ in a) air and b) nitrogen.

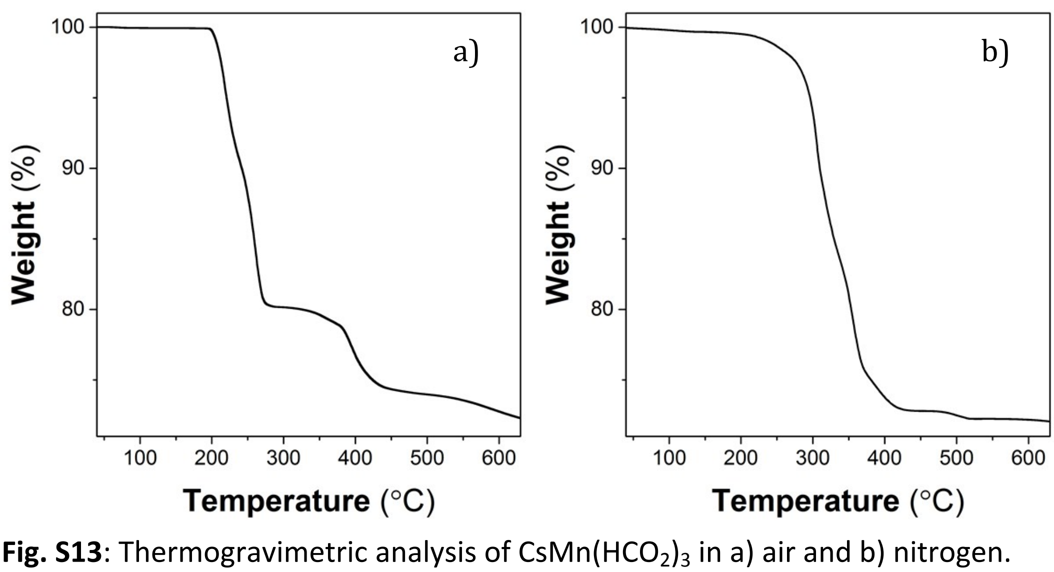

Fig. S13: Thermogravimetric analysis of $CsMn(HCO_2)_3$ in a) air and b) nitrogen.